Construction of GPx Active Centers on Natural Protein Nanodisk/Nanotube: A New Way to Develop Artificial Nanoenzyme

Chunxi Hou,[†] Quan Luo,[†] Jinliang Liu,[‡] Lu Miao,[†] Chunqiu Zhang,[†] Yuzhou Gao,[†] Xiyu Zhang,[†] Jiayun Xu,[†] Zeyuan Dong,[†] and Junqiu Liu[†,*]

[†]State Key Laboratory of Supramolecular Structure and Materials, College of Chemistry, Jilin University, 2699 Qianjin Street, Changchun 130012, China and [‡]College of Plant Science, Jilin University, 5333 Xi'an Road, Changchun 130062, China

ABSTRACT

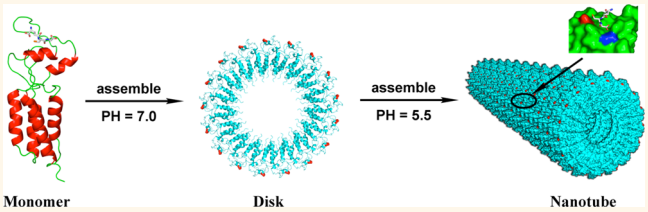

Construction of catalytic centers on natural protein aggregates is a challenging topic in biomaterial and biomedicine research. Here we report a novel construction of artificial nanoenzyme with glutathione peroxidase (GPx)-like function. By engineering the surface of tobacco mosaic virus (TMV) coat protein, the main catalytic components of GPx were fabricated on TMV protein monomers. Through direct self-assembly of the functionalized viral coat proteins, the multi-GPx centers were installed on these well-defined nanodisks or nanotubes. With the help of muti-selenoenzyme centers, the resulting organized nanoenzyme exhibited remarkable GPx activity, even approaching the level of natural GPx. The antioxidation study on subcell mitochondrial level demonstrated that virus-based nanoenzyme exerted excellent capacity for protecting cell from oxidative damage. This strategy represents a new way to develop artificial nanoenzymes.

KEYWORDS: tobacco mosaic virus · artificial enzyme · self-asselmbly · nanodisk · nanotube · glutathione peroxidase

There is currently intense interest in the use of natural occurring nanocomponents for a wide range of material and technological applications. Among the known biological nanocomponents, the virus has recently become a versatile tool for nanomaterial and nanodevice design. Taking advantage of anisotropic structure and stability, various viruses including filament, fiber, cage, and tube-like viruses have been explored as building blocks in catalyst,[1] nanoscale electronics,[2] biomineralization,[3] energy storage,[4] light harvesting,[5] and other biomedical researches.[6] Among the viruses, tobacco mosaic virus (TMV) has been investigated extensively because TMV has many unique characteristics for nanomaterial design. Specifically, TMV comprises 2130 coat proteins which can assemble into a 300 nm long tubular virus with a diameter of 18 nm and a 4 nm center channel. It can be produced in large quantities through propagations of the intact virus in plants or genetic expression of the coat protein. More importantly, the coat protein-induced assemblies can be specially functionalized through chemical and genetic modifications.[7] For example, using a hexahistidine modified TMVcp derivative, Bruckman *et al.* figured out a series of assembly routes to achieve amusing disks, hexagonally packed arrays of disks, stacked disks, helical rods and elongated rafts. Utilizing TMV disks, this group fabricated exquisite 22 nm gold nanoparticle rings with a controllable loading of central nanoparticles.[8,9] Modifications of TMV coat proteins not only could produce advanced 2D or 3D order structures, but also could bring out inspiring bionic materials for biomedical applications.[10−13]

For mimicking the process of photosynthesis, Miller *et al.* created very smart light harvesting systems by relocating the N- and C-termini of TMV coat protein to the channel and installing thousands of donor- and acceptor-chromophores for energy transfer.[14] For mimicking the nature way that smooth muscle cells (SMCs) align perpendicular to the blood vessel length, Lin and co-workers made the growth of SMCs in the 2D strip patterns of TMV, which can form in a concentration-dependent manner.[15] Recently,

* Address correspondence to junqiuliu@jlu.edu.cn.

Received for review May 22, 2012 and accepted September 19, 2012.

Published online September 19, 2012
10.1021/nn302270b

a major topic in bionic research is to assemble multiple enzymatic centers on large protein structures. Notably, an important report introduced that assembled catalysts on protein assemblies such as M13 virus mediated photocatalytic nanostructures could improve structural durability and facilitate recycle.[16] So far, TMV virus has been used to develop such advanced materials by the assembly of Pd nanoparticle catalysts on it;[17] however, TMV disks or tubes have not been explored to assemble multiple catalytic centers of natural enzymes, which will strengthen the utility of multiple natural enzymes.

In fact, multiple catalytic centers on protein assemblies could favor controllable catalysis, fabrication of biosensor, and synergistic catalysis in biological processes. Komatsu *et al*. demonstrated that α-glucosidase functionalized protein tubes possessed exquisite and facile control on catalysis to capture substrate fluorogenic glucopyranoside and release α-D-glucose in a protein channel.[18] Also, peroxidase assemblies could be plugged in the porous substrate (less than 100 nm) on the electrode to make biosensors.[19] Furthermore, multiple enzymes on the nanoscale assemblies such as highly efficient peroxidase-functionalized nanoparticles can exhibit a synergistic or cooperative effect in catalysis.[20] Definitely, such enzyme assemblies provide stable locations for an enzyme, exposed catalytic sites and appropriate enzyme−substrate interactions during the catalytic reaction.

However, to assemble catalytic centers or multiple enzymes on protein templates with high orientation is a challenging work. Comparably, some successes have been achieved toward the use of DNA as scaffold to assemble catalytic centers.[21] The organization of glucose oxidase (GOx)/horseradish peroxidase (HRP) on the DNA origami tiles, and heterogeneous enzymes or cofactor-enzyme cascades on hexagon-like DNA scaffolds, demonstrated that DNA templates could provide high efficiency and precise positions to organize enzymes.[22,23] In comparison, it is difficult to build up multiple catalytic centers on large protein assemblies owing to the lack of efficient methods. Fortunately, it becomes possible since enzyme simulation technique appears as a powerful tool which has successfully provided many enzyme mimics.

Glutathione peroxidase (GPx, EC 1.11.1.9) is the first discovered selenoenzyme in mammalian, which efficiently catalyzes the reduction of harmful hydroperoxides by the reductive substrate glutathione (GSH), and plays an important role in protecting the biomembranes and other cellular components from oxidative damage in the antioxidant defense system. In recent years, there are increasing interests in mimicking the functions of this important antioxidant enzyme. Using the concept of synergy of the recognition and catalysis, many successful GPx models have been constructed. Examples include the designed GPx mimics in which selenium catalytic centers have been introduced into the existing or artificially generated substrate binding sites on single proteins.[24] These naturally existing proteins are conferred to be ideal starting points to engineer novel enzyme functions. However, the design of artificial GPx systems on nanoscale protein aggregates is one of the great challenges. Very recently we developed a novel way to construct GPx active centers on organic nanotubes by the self-assembly of "supermolecular amphiphiles" and demonstrated that the strategy of self-assembly has a great potential for the construction of artificial nanoscale enzymes.[25] Inspirited by these successful examples, we wondered whether we could develop an enzymatic protein nanodisk/nanotube based on natural protein aggregates by combining an artificial seleno-enzyme design with naturally evolved self-assembly. For this challenging design, we selected genetically expressed TMV coat protein (TMVcp, a cysteine-free mutant with the replacements of Cys27 and Cys123 by glycines) as the starting protein because of its high yield, stable aggregates, and highly resolved crystal structure.

Herein we report a novel construction of artificial nanoenzyme with glutathione peroxidase (GPx)-like function. By combining artificial seleno-enzyme design concept of the synergy of substrate recognition and catalysis with computer simulation, the main catalytic components of GPx were fabricated on TMV protein monomers. Through direct self-assembly of the functionalized viral coat proteins, the multi-GPx centers were installed on these well-defined nanodisks or nanotubes. The resulting organized nanoaggregates exhibited remarkable GPx activities, even approaching the level of natural GPx. The antioxidation study on the subcell mitochondrial level demonstrated that the virus-based nanoenzyme exerted excellent capacity for protecting cell from oxidative damage. The plant virus-derived nanoenzymes have low immune responses in mammal, providing the potential pharmaceuticals for the antioxidative diseases such as aging and cardiovascular disease.

RESULTS AND DISCUSSION

Construction of Catalytic Center of GPx on TMVcp. At the active site of natural GPx,[26] a catalytic moiety, selenocysteine (Sec) and a specific binding site for substrate GSH present as a shallow groove on the enzyme surface, and the substrate GSH can be stabilized mainly by two arginines (Arg 57, Arg 103) residues. After carefully modeling the surface of TMVcp with the assistant of computer simulations, a depression on the surface of TMVcp was found similar to the catalytic site of natural GPx (Schemes 1 and 2), which may be accessible to the substrate GSH and promote the substrate recognition and catalysis. On this assumable substrate binding site, Ser142, a more exposed position on their surface was selected as an alternative site to install the GPx catalytic

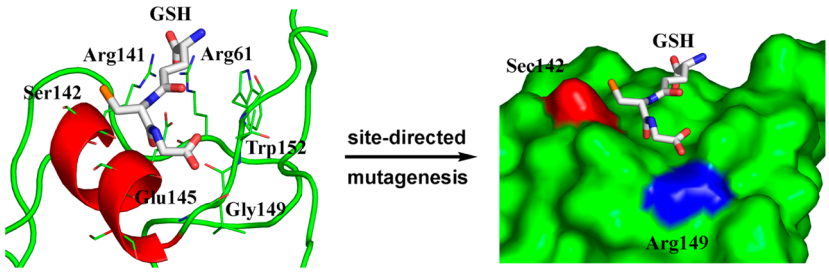

Scheme 1. Computer simulation of TMVcp (a cysteine-free mutant) to construct the GPx mimic Se-TMVcp142Cys149Arg (substituting Ser142 and Gly149 of TMVcp by selenocysteine and arginine, respectively). Site142 is located in α helix of TMVcp which is an ideal alternative to incorporate selenocysteine, the natural catalytic group of GPx. Arg141 and Arg149 (blue, point mutation) could form salt bridges with GSH to enhance the substrate binding and stabilize the reactive intermediates. And relative important amino acids Arg141, Arg61, Glu145, Gly149, and Trp152 involved in binding and catalysis are presented on the ribbon. Through molecular docking, substrate GSH can bind to the surface depression shallow and react with selenocysteine (red, point mutation)

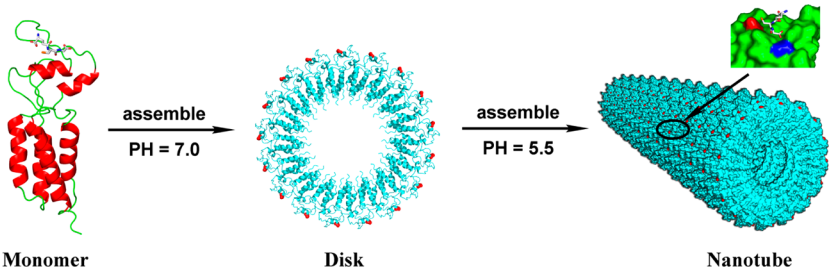

Scheme 2. Assembly of GPx mimic Se-TMVcp142Cys149Arg into artificial nanoenzyme. Se-TMVcp142Cys149Arg is designed by computer analysis, and acts as an artificial GPx mimic after expression in a cysteine auxotrophic system. Under different conditions (pH 5.5 and pH 7.0), GPx active centers can be successfully exhibited on the outer surface of Se-TMVcp142Cys149Arg nanodisks and nanotubes as 34 monomers and more than a thousand monomers, respectively.

moiety, Sec (Schemes 1 and 2). Moreover, the displacement of glycine by arginine at 149 could contribute to GPx activity by forming a salt bridge with substrate GSH and could result in the shift from selenosulfide (ESeSG) to selenolate (ESe-), which is a key rate-determining step in the catalytic cycle.

For installing the catalytic moiety selenocysteine, the Ser142 of TMVcp was first replaced with a cysteine residue and then substituted with the catalytically essential Sec residue using a cysteine auxotrophic system.[25] The Se-TMVcp142Cys149Arg was purified by DEAE anion exchange chromatography and thiopropyl-sepharose 6B-based affinity chromatography, and was characterized with mass spectrometry, polyacrylamide gel electrophoresis, selenium content analysis, and circular dichroism. As shown in Figure 1, after genetic mutation and selenium incorporation in a cysteine auxotrophic expression system, Se-TMVcp142Cys and Se-TMVcp142Cys149Arg exhibited nearly the same CD spectra, which suggested the similar secondary structures of wild TMVcp, Se-TMVcp142Cys, and Se-TMVcp142Cys149Arg. The determination of selenium content showed that there was 0.96 equivalent of selenium per mole Se-TMVcp142Cys149Arg, demonstrating the incorporation of Sec residue (Table 1). Mass spectrometry and ICP analysis gave us further proofs for efficient Sec incorporation (see Supporting Information, Figure 4S and Table 1S).

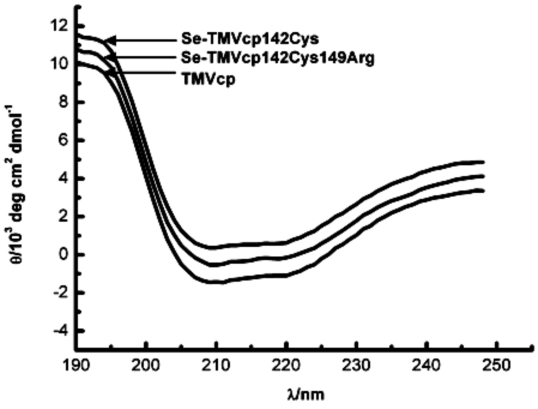

Figure 1. CD spectra of wild type TMVcp, Se-TMVcp142Cys, and Se-TMVcp142Cys149Arg monitored from 190 to 250 nm. Prior to CD measurement, Se-TMVcp142Cys149Arg, Se-TMVcp142Cys, and wild type TMVcp were exchanged into 50 mM PB buffer (pH7.0) containing 150 mM NaCl, 1 mM EDTA, and adjusted to a final concentration of 0.15 mg/mL. Background spectra in the absence of protein were measured and subtracted.

Assembly of GPx Mimic of TMVcp Mutant. For assessing the self-assembly capacity of Se -TMVcp142Cys149Arg, the assembly behaviors of Se-TMVcp142C149Arg mediated by pH values were detected by AFM and TEM. As CD analysis indicated (Figure 1), Ser142Sec substitution did not alter the secondary structure of the protein domain. It implied that the genetic operation for

TABLE 1. GPx Activities of Se-TMVcp142Cys149Arg and Other GPx Mimics

catalyst	substrate	activity[a] (one disk or natural assemblies) (μmol·min^{-1}· μmol^{-1})	activity (one monomer) (μmol·min^{-1}·μmol^{-1})	selenium content (M/M per subunit)
TMVcp[b]	H_2O_2	ND	ND	0
TMVcp142Cys[c]	H_2O_2	3.4 ± 0.1	0.1 ± 0.03	0
Se-TMVcp142Cys[d]	H_2O_2	6320 ± 13.5	185.9 ± 0.41	0.95
Se-TMVcp142Cys149Arg[e]	H_2O_2	9356 ± 17.2	275.2 ± 0.50	0.96
Ebselen	H_2O_2	1.02[f]	1.02	1.0
native GPx (rabbit liver)	H_2O_2	5780[g]	1445	1.0

[a] The GPx activity for the reduction of H_2O_2 catalyzed by Se-TMVcp142Cys149Arg was determined in the following mixture: 1 mM EDTA, 1 mM GSH, 1U GSSG reductase, 0.25 mM nicotinamide adenine dinucleotide phosphate (NADPH) and 10—300 nM of enzyme mimics. The reaction was initiated by the addition of 0.5 mM H_2O_2 and monitored from the decrease of NADPH absorption at 340 nm. The activity unit is defined as the amount of enzyme that consumes 1 μmol of NADPH per min. The specific activity is expressed as U·μmol^{-1} or μmol·min^{-1}·μmol^{-1}.. [b] TMVcp: a cysteine-free mutant with replacements of Cys27 and Cys123 with glycines. ND = no detection. [c] TMVcp142Cys: a mutant with single cysteine incorporated at site142 of TMVcp. [d] Se-TMVcp142Cys: expression of TMVcp142Cys-containing plasmid in a cysteine auxotrophic system. [e] Se-TMVcp142Cys149Arg: expression of TMVcp142Cys149Arg-containing plasmid in a cysteine auxotrophic system. [f] GPx activity of ebselen was determined under the same conditions in this study. [g] Activity value of GPx analogue is from ref 27. GPx activity is expressed as total activities of rabbit liver GPx tetramers.

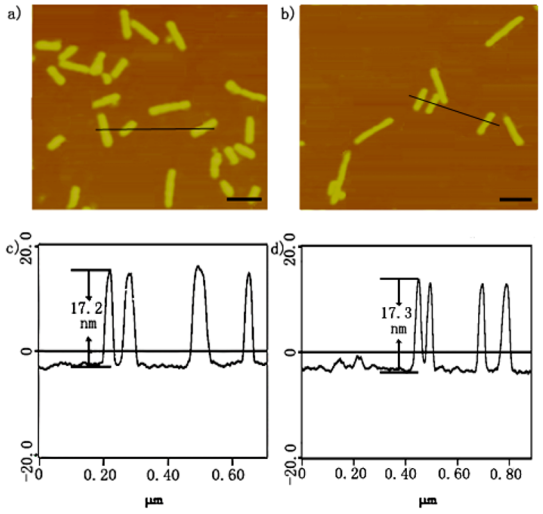

Figure 2. AFM images of tubes assembled from Se-TMVcp142Cys149Arg and TMVcp. (a) Assembly of TMVcp at a concentration of 60 μM. (b) Assembly of Se-TMVcp142Cys149Arg at a concentration of 60 μM. (c,d) Height curves of assembled tubes corresponding to panels a and b. Scale bars in panels a and b are 100 nm.

TMVcp may not affect the assembly behaviors of monomer proteins. To avoid the aggregation induced by chemical ligation of selenocysteine, 1 mM DTT was added. As shown in Figure 2a,b, Se-TMVcp142Cys149Arg could spontaneously assemble into the nanotubes in acidic buffers that are much like those assembled from the wild-type proteins, and the length of the tube can reach several micrometers. The TMV nanotubes can exist stably in a wide pH range. The height of the tubes of Se-TMVcp142Cys149Arg was measured as 17.1 ± 0.5 nm which is well near to the theoretical value of 18 nm if the interaction of tip and protein was ruled out (Figure 2c,d. Furthermore, the morphology of the assembly can be altered by the pH change. When changing pH value of the buffer to neutral, disk-like assemblies were generated with the height of 4.6 ± 0.2 nm which matched well to the practical disks assembled from 34 protein monomers (Figure 3). AFM analysis gave us further evidence for the assembled nanostructures under concentration control (see Supporting Information, Figure 5S).

GPx Activity of GPx Mimic of TMVcp Mutant. Like natural GPxs, selenium-containing TMVcp mutants can catalyze the reduction of H_2O_2 by GSH. Significantly, the GPx activity of one selenium center of Se-TMVcp142Cys was found to be 185.9 U·μmol^{-1}, and the activity of Se-TMVcp142Cys149Arg further increased up to 275.2 U·μmol^{-1} after the arginine was incorporated close to the catalytic site, while no GPx activity was observed in wild-type protein TMVcp, and only a slight GPx activity (0.1 U·μmol^{-1}) has been detected in cysteine mutant TMVcp142Cys (Table 1). This result confirms that the GPx activity observed is derived from the Sec residue introduced at the GSH binding site of Se-TMVcp142Cys149Arg. The activity of 275.2 U·μmol^{-1} is remarkable, because it is only from one selenium center. Before or after the disk assembly at pH 7.0, the determinations of GPx activities of Se-TMVcp142Cys149Arg gave out the consensus results. Thus, the increase of activities in assemblies is linearly dependent on the number of monomers. As shown in Table 1, the Se-TMVcp142Cys149Arg with disk-like morphology consists of 34 active centers in 34 protein monomers, the whole disk-like assembly of which shows significantly high GPx activity (9356 ± 17 U·μmol^{-1}) approaching that of the natural GPx, it is at the same order of magnitude as some native GPxs (for example, 5780 U·μmol^{-1} for rabbit liver GPx tetramer with 4 selenium centers)[27] and approximately 9173 times higher than that of the well-studied GPx mimic ebselen (1.02U μmol^{-1}). When we refer the tube as a nanoenzyme, the GPx activity of whole nanotube exhibits extremely high activity, obviously exceeding native GPxs, for example, assuming 2000 coat proteins in one tube, the whole activity of a nanotube goes up to 550400 U·μmol^{-1}.

To evaluate GPx mimic Se-TMVcp142Cys149Arg, the catalytic mechanism for the reduction of hydrogen

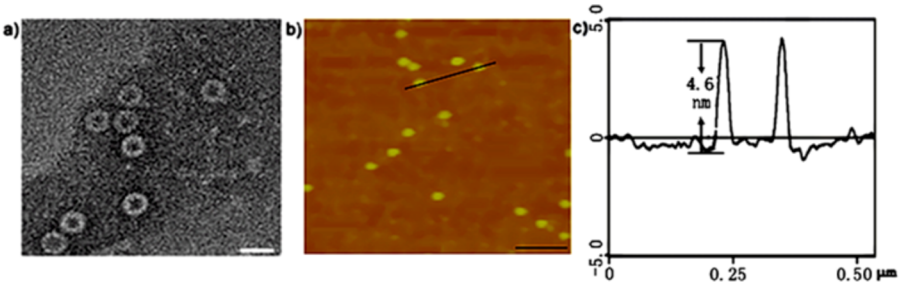

Figure 3. TEM and AFM images of disks assembled from Se-TMVcp142Cys149Arg. (a) TEM image of Se-TMVcp142Cys149Arg disks which were assembled by exchanging buffers from pH 8.0 to pH 7.0. Samples were taken after equilibrium for above 40 h. (b) AFM image of Se-TMVcp142Cys149Arg disks. (c) Height curve of disk assemblies from panel b. The scale bars in panels a and b are 20 nm and 100 nm, respectively.

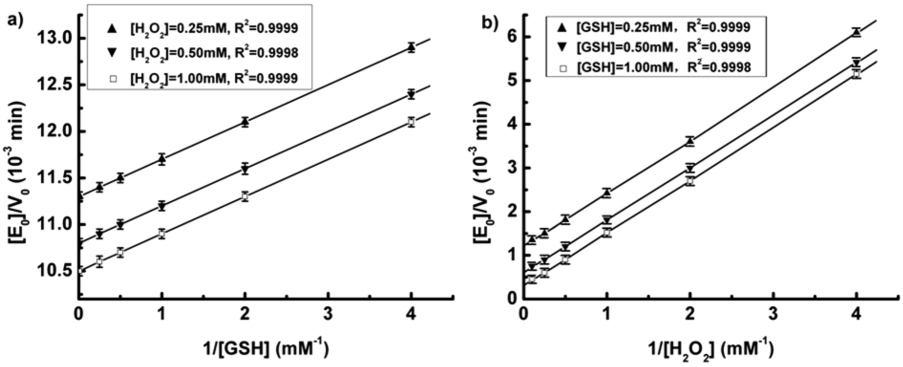

Figure 4. Double reciprocal plots of H_2O_2 reduction by GSH in the presence of GPx mimic of monomer Se-TMVcp142Cys149Arg. (a) $[E_0]/V_0$ *versus* 1/[GSH] at $[H_2O_2]$ = 0.25 mM (▲), 0.50 mM (▼), and 1.00 mM (□). (b) $[E_0]/V_0$ *versus* 1/$[H_2O_2]$ at [GSH] = 0.25 mM (▲), 0.50 mM (▼), and 1.00 mM (□).

TABLE 2. Apparent Kinetic Parameters[a] for H_2O_2 Reduction by GSH Catalyzed by Se-TMVcp142Cys149Arg (One Active Center)

$[H_2O_2]$ (mM)	k_{cat} (min^{-1})	$K_M^{H_2O_2}$ ($\times 10^{-4}$ M)	$k_{cat}/K_M^{H_2O_2}$ ($\times 10^6$ M^{-1} min^{-1})	[GSH] (mM)	k_{cat} (min^{-1})	K_M^{GSH} ($\times 10^{-3}$ M)	k_{cat}/K_M^{GSH} ($\times 10^5$ M^{-1} min^{-1})
0.25	91.54 ± 4.51	0.36 ± 0.02	2.54 ± 0.11	0.25	877.2 ± 40.22	1.09 ± 0.04	8.05 ± 0.37
0.50	95.37 ± 4.82	0.37 ± 0.05	2.58 ± 0.12	0.50	1851 ± 80.60	2.30 ± 0.01	8.05 ± 0.36
1.00	98.52 ± 5.71	0.38 ± 0.03	2.59 ± 0.15	1.00	2778 ± 130.5	3.33 ± 0.01	8.34 ± 0.41

[a] The data in the table were calculated from the plots in Figure 4 with the following equation:

$$\frac{v_0}{[E_0]} = \frac{k_{cat}[GSH][H_2O_2]}{K_M^{GSH}[H_2O_2] + K_M^{H_2O_2}[GSH] + [GSH][H_2O_2]}$$

peroxide by GSH catalyzed by Se-TMVcp142Cys149Arg was studied. The typical Michaelis−Menten kinetics was observed (Figure 4). Double reciprocal plots of the initial velocities *versus* the concentrations of the substrates generate a group of parallel lines, indicating at least one covalent intermediate during catalysis, which is the characteristic of a ping−pang mechanism. Furthermore, treatment of the Se-TMVcp142Cys149Arg with excess iodoacetate resulted in complete loss of GPx activity, indicating an enzyme bound selenol during the catalysis. These facts are in good agreement with those of natural GPx.

To obtain the insight into the steady kinetics, catalytic parameters were calculated according to the kinetic equation (Table 2). The pseudo-first-order rate constant k_{cat} and the apparent Michaelis constant K_M at 0.5 mM GSH were counted to be 1.85 min^{-1} and 2.30 × 10^{-3} M, respectively. The apparent second-order rate constant k_{cat}/K_M of Se-TMVcp142Cys149Arg was found to be 8.05 × 10^5 M^{-1} min^{-1}. It is an obvious high bimolecular reaction rate with respect to the absence of natural GSH binding site for TMVcp. Although it is 2 orders of magnitude less than that of natural GPx, such as phospholipid hydroperoxide glutathione peroxidase (2.7 × 10^7 M^{-1} min^{-1}),[28] it approaches that of GPx mimic seleno-GST-SOD and is 2 orders of magnitude higher than that of GPx mimic, Se-4A4 (4.5 × 10^3 M^{-1} min^{-1}).[29] Considering that the catalytic parameters were calculated from only one selenium center, the kinetic study also confirmed that the assemblies

with multi-GPx centers were installed with high catalytic efficiency.

Bioantioxidant Capacity of GPx Mimic of Se-TMVcp142Cys149Arg Disks. Se-TMVcp142Cys149Arg exhibits therefore not only significant high GPx activity but also the ability to assemble into disks or tubes. Modified TMV disks or tubes have been proven to be useful in the fabrication of molecular devices. For instance, TMV tubes functionalized with oligo-aniline were successfully integrated into biosensors for detection of volatile organic compounds.[13] To obtain stable enzyme assemblies for potential application in biosensors or biomaterials such as enzymatic detection of radical oxygen species (ROS), in this study, the Se-TMVcp142Cys149Arg disks were subjected to glutaraldehyde cross-linking and SEC-HPLC purification. DLS research revealed that the fixed Se-TMVcp142Cys149Arg disks were not obviously disaggregated after three freeze−thaw cycles, demonstrating that glutaraldehyde was appropriate to fix the Se-TMVcp142Cys149Arg disks (see Supporting Information, Figure 6S). Prior to the study of Se-TMVcp142Cys149Arg disks in protecting mitochondria against oxidative damage, we fractionated the fixed Se-TMVcp142Cys149Arg disks and tubes by SEC-HPLC (see Supporting Information, Figure 7S). As a result, HPLC profile supported that the cross-linked Se-TMVcp142Cys149Arg disks and tubes had good stabilities toward the elution during HPLC. TEM of the purified tubes (Figure 5g) displayed disperse tubes with various lengths. Notably, the resulting morphology of disks indicated a diameter of 18 m and a width of 4.6 nm, as shown in Figure 5d−f, which was in agreement with double-layer disk (Figure 5a−c, based on the crystal structures).

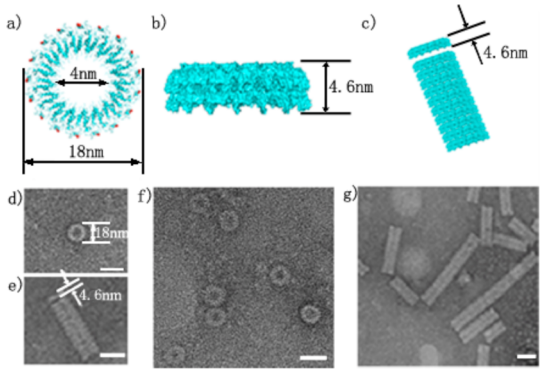

Figure 5. Theoretical pictures made by software pymol and TEM images of Se-TMVcp142Cys149Arg disks and tubes purified by SEC-HPLC. (a) Vertical view of Se-TMVcp142Cys149Arg disks. (b) Side view of Se-TMVcp142Cys149Arg disks. (c) Transition of Se-TMVcp142Cys149Arg disks to Se-TMVcp142Cys149Arg tubes. (d,f) TEM image of purified disks. (e) TEM image of disk-to-tube transitions. (g) TEM image of purified Se-TMVcp142Cys149Arg tubes.

To further evaluate the antioxidative capacity of the artificial nanoscale selenoenzymes, their ability to protect mitochondria against oxidative damage was measured. Once the mitochondria are damaged in the presence of oxidative stress, the integrity of mitochondria would decrease and swelling would happen, resulting in the decrease of absorbance at 520 nm. Considering the 3D morphology, the two-layer disk-like structures of GPx mimic Se-TMVcp142Cys149Arg are more uniform and fit in width, the small and regular morphology of which cannot only favor the catalytic reaction, but also facilitate the cell phagocytosis and other biomedical effect. During the mitochondria swelling assay, the absorbance at 520 nm of the undamaged controls both decreased slightly (Figure 6a,b), in contrast, when the samples incubated with sulfate/ascorbate, oxidative damage of mitochondria was induced. When the GPx mimics of Se-TMVcp142Cys149Arg disks were added to the reaction system, the absorbance of mitochondria at 520 nm was decreased which indicated Se-TMVcp142Cys149Arg disks as protecting agents displaying a concentration-dependent effect. Notably, Se-TMVcp142Cys149Arg had the same protection effect at only 1/80 concentration of 2-selenocyclodextrin (2-SeCD), while the GPx activity of Se-TMVcp142Cys149Arg was only nearly 40 folds that of 2-SeCD (Figure 6b). The subcell antioxidative experiments demonstrated that TMV-based nanoselenoenzyme had a

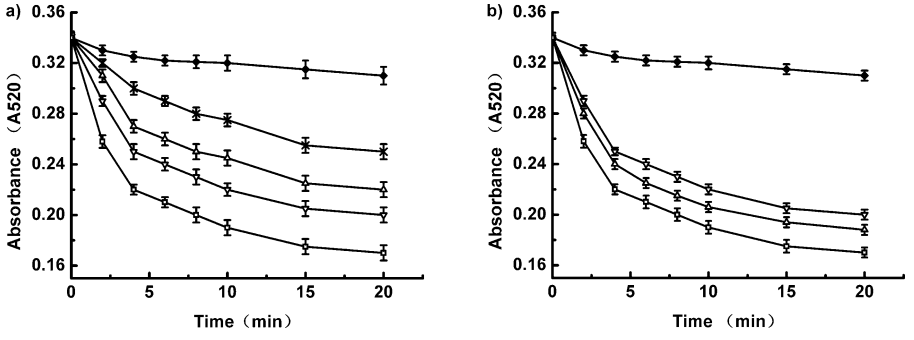

Figure 6. Determination of the mitochondria swelling in the presence of GPx mimics of Se-TMVcp142Cys149Arg disks and 2-SeCD. (a) Mitochondria swelling in the presence of Se-TMVcp142Cys149Arg disks at various concentrations of 0 μM (□), 0.025 μM (▽), 0.050 μM (△), 0.100 μM (×), and control with no oxidants (♦). (b) Comparison of mitochondria swelling in the presence of Se-TMVcp142Cys149Arg disks (▽) at 0.025 μM, 2-SeCD (△) at 2 μM, and controls with no GPx mimics (□) and with no oxidants (♦).

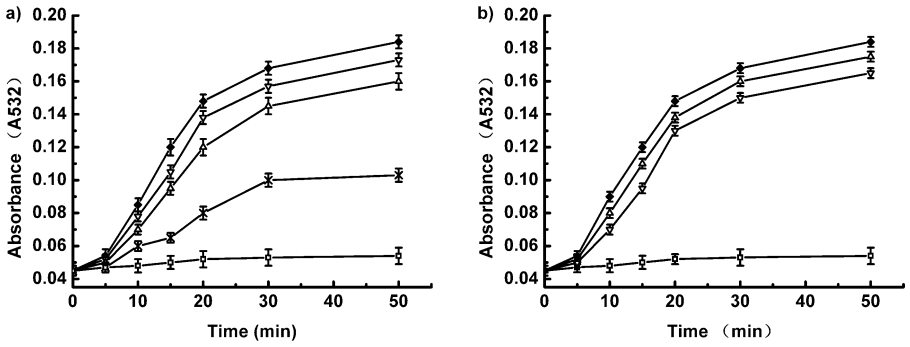

Figure 7. Determination of lipid peroxidation in the presence of GPx mimics of Se-TMVcp142Cys149Arg disks and 2-SeCD. (a) Inhibition of MDA content over times by Se-TMVcp142Cys149Arg disks at various concentrations of 0 μM (♦), 0.025 μM (▽), 0.050 μM (△), 0.100 μM (×) and control of no oxidant (□). (b) Inhibition comparisons of MDA content over times by Se-TMVcp142Cys149Arg disks (▽) at 0.025 μM and 2-SeCD (△) at 2 μM, no GPx mimics (♦), control of no oxidant (□).

nice biocompatibility and high ability for protecting the cell against oxidative damage.

The lipid peroxidation of mitochondria was assayed in the presence of Se-TMVcp142Cys149Arg disk using the thiobarbituric acid (TBA) assay following the procedure described previously.[26] The final product of the free-radical-mediated lipid peroxidation is malondialdehyde (MDA), which could form adducts with TBA, leading to intense absorbance at 532 nm. As shown in Figure 7, the MDA accumulation was inhibited by Se-TMVcp142Cys149Arg disks in a concentration-dependent manner. Furthermore, Se-TMVcp142Cys149Arg disks exhibited similar protective effect to 2-SeCD at only 1/80 fold concentration of 2-SeCD.[42] In comparison with monomer Se-TMVcp142Cys149Arg, the assemblied structure could prevent the selenium-caused gathering between monomer Se-TMVcp142Cys149Arg, and thus contribute to the highly protective ability. The above fact highlights the importance of disk morphology in contributing to the elimination of the radical oxidant. This may be ascribed to the many selenocysteines exposed on the surface of Se-TMVcp142Cys149Arg disks, which could provide much opportunity to facilitate radical oxidant approach.

CONCLUSION

In conclusion, GPx catalytic center was successfully constructed on TMV disks or tubes by a novel strategy combining computer simulation, cysteine auxotrophic expression with self-assembly approach. The nanoselenoenzyme, that was assembled from Se-TMVcp142Cys149Arg (a TMVcp mutant with catalytic selenium incorporated site142 and binding site arginine incorporated at site149) showed very high efficient GPx activity even approaching the level of natural GPx. Thus the combination of multi-approaches cannot only incorporate the catalytic moiety, install the recognition site to the natural nanoscaffolds, but also ensure the disk assembly showing high activity. The combined strategy could avoid denaturing of the protein compared with other approaches for enzyme simulation, such as chemical modification. Notably, the Se-TMVcp142Cys149Arg disks exhibited excellent stability following the glutaraldehyde cross-linking, and its stability significantly widens its range in biological applications. Also, the disk or tube-like artificial nanoenzymes may provide a feasible application in biosensors because of the excellent catalysis and convenient recovery. Compared with other artificial selenoenzymes, the nanoselenoenzymes exhibit nice biocompatibility and excellent antioxidant capacity in the protection of mitochondria against swelling and lipid peroxidation. We hope that the virus derived, selenium-containing, and self-assembled nanoenzymes will be a versatile material for applications in biosensors and biomedicine. The strategy may also serve as a platform to generate other multifunctional enzymes for further application in nanomaterials or nanodevices.

MATERIALS AND METHODS

Plasmid pET20b containing the TMV coat protein gene (pET-TMV) was a gift from Professor M. B. Francis (University of California, Berkeley, USA). The cysteine auxotrophic strain was a gift from Professor A. Bock (University of Munich, Germany). Phenylmethanesulfonyl fluoride (PMSF), glutathione reductase (GR), reduced glutathione, and nicotinamide adenine dinucleotide phosphate (NADPH) were purchased from Sigma (Germany). PrimeSTAR HS DNA polymerase, Agarose Gel DNA Purification Kit, and DNA Fragment Purification Kit were obtained from Takara (Japan). Dpn I was a product of Fermentas. Sephadex G25 and G75 were purchased from Amersham Pharmacia Biotech (Uppsala, Sweden). All the other reagents were obtained from Beijing Chemical Plant and of analytical grade.

Construction of Catalytic Center of GPx on TMVcp. Computer simulation of TMVcp was conducted according to the method described by Zhang *et al.*[30] The catalytic center and binding site of GPx were searched in the crystal structure of TMVcp using computer simulation software pymol.[31] Subsequently, the fitting value was confirmed by program proposed.[32−36]

The original TMV coat protein gene encodes two cysteines including the sites of 27 and 123, which are the buried inherit cysteine of wild TMV and the mutant RNA binding site coming from construction by donor, respectively. To avoid influencing

the analysis in GPx activity, they were all substituted with glycines through point mutations, and named TMVcp. For point mutation at site 27, primers used were PU27 (5′-AACCTGGGCACCAATGCGCT-3′), and PD27 (5′- GCATTGGTGCCCAGGTTAAT-3′); for point mutation at site 123, primers used were PU123 (5′-TGGCGATTCGCGGTGCCATC-3′) and PD123 (5′-GGCACCGCGAATCGCCACGG-3′). According to structure design by computer analysis, single cysteine was incorporated into site142 of TMVcp to obtain TMVcp142Cys using the primers PU142 (5′- GTTGCAGCTTTGAAAGCAG-3′) and PD142 (5′-TCAAAGCTGCAACGGTTATA-3′). Further more, another mutant TMVcp142Cys149Arg was obtained by PCR using primers PU149 (5′-GCAGCCGCCTGGTGTGG-3′) and PD149 (5′-ACCAGGCGGCTGCTGCT-3′) with the template TMVcp142Cys. Two plasmids encoding TMVcp142Cys and TMVcp142Cys149Arg were transformed into BL21cysE51 competent cells and stored at 4 °C until the tag-free expression in M9 media following a procedure described previously with modifications.[37]

Expression of GPx Mimic of TMVcp Mutant. For substituting cysteine with selenocysteine in TMVcp142Cys149Arg and TMVcp142Cys to generate Se-TMVcp142Cys149Arg and Se-TMVcp142Cys, the aimed strain BL21cysE51 was used for cysteine auxotrophic expression, which was constructed by insertion of *cysE51* allele from JM39/2 into *E.coli* strain BL21. Monoclonal cells containing genes of TMVcp142Cys149Arg and TMVcp142Cys were cultured in 20 mL of LB medium including ampicillin (50 μg/mL) and kanamycin (50 μg/mL) overnight. The cultured cells were inoculated into 1.0 L M9 culture medium to reach an OD_{600} of 0.1 consisting of ampicillin (50 μg/mL), kanamycin (50 μg/mL), and inorganic salts-Na_2HPO_4 (6.0 g/L), KH_2PO_4 (3.0 g/L), NaCl (0.5 g/L), NH_4Cl (0.2 g/L), $MgSO_4$ (0.241 g/L), 20 normal amino acids (each one at 100 mg/L), and glucose (20 g/L). When the cultured cells grew to OD_{600} of 1.0, chloramphenicol was added to a final concentration of 10 μg/mL and incubated for 10 min. Immediately IPTG was added to a concentration of 1 mM, and the mixture was incubated for 20 min. The sediment cells were acquired by centrifugation at 8000 rpm and washed three times with cold 50 mM phosphate buffer (containing 150 mM NaCl). The cleaned cells were transferred to M9 production medium containing ampicillin (50 μg/mL), kanamycin (50 μg/mL), 400 μg/mL rifampicin, 50 mg/L DL-selenocysteine, and 20 normal amino acids (each one at 100 mg/L), four kinds of bases (each one at 50 mg/L), biotin (100 μg/L), glycerol (4,v/v), glucose (20 g/L), and inorganic salts including K_2HPO_4 (3.0 g/L), NH_4Cl (1.0 g/L), NaAc (2.0 g/L), $CaCl_2$ (10.0 mg/L), MgAc (429.0 mg/L), and $FeCl_2$ (3.6 g/L). The culture flasks were agitated at a low velocity of 120 rpm to reduce the toxicity of DL-selenocysteine. During the culture period, SDS-PAGE was used to monitor the expression level of Se-TMVcp142Cys149Arg and Se-TMVcp142Cys. After 7 h of culture, cells were harvested by centrifugation at 8000 rpm and stored at −80 °C.

Se-TMV1cp142Cys149Arg and Se-TMV1cp142Cys were determined to evaluate the selenium content. The protein concentrations were determined by the Bradford method using BSA as a standard. The selenium content was determined by titration of the sodium borohydride-reduced protein with 5,5-dithiobis(nitrobenzoic acid) as described.[29]

To evaluate the secondary structure change between wild TMVcp, Se-TMVcp142Cys, and Se-TMVcp142Cys149Arg, circular dichroism (CD) spectra were carried out for comparison of their structures at room temperature.[38,39] Prior to CD measurement, Se-TMVcp142Cys149Arg, Se-TMVcp142Cys, and wild type TMVcp were exchanged into 50 mM PB buffer (pH7.0) containing 150 mM NaCl, 1 mM EDTA, and adjusted to a final concentration of 0.15 mg/mL. Background spectra in the absence of protein were measured and subtracted.

Assembly of GPx Mimic of TMVcp Mutant. Before assembly, Se-TMVcp142Cys149Arg was exchanged into 20 mM Tris-HCl, pH 8.0 overnight to obtain the monomer Se-TMVcp142Cys149Arg, meanwhile, size-exclusion HPLC chromatography was used to monitor the procedure. For assembly into the tube, monomer solution (50 μL) was dialyzed (8000 kDa cutoff membrane) against 50 mM PB buffer (pH5.5) containing 1 mM EDTA at room temperature. For assembly into the disk, monomer solution (50 μL) was dialyzed against 50 mM PB buffer (pH7.0) containing 1 mM EDTA for 4 days. Prior to determination, the sample (5 μL/sample) was added onto the silicon plate pretreated with hydrogen peroxide/vitriol and adsorbed for 5 min. Then, samples were subjected to atomic force microscopy (AFM) scan following rinsing for three times and drying under N_2 blowing. All the assembled samples were assayed by AFM on tapping mode. The lengths of tubes and disks were statistically calculated by five-time AFM measures per dried drib samples.

Transmission electron microscopy (TEM) images were recorded using a FEI Tecnai 12 transmission electron microscope with 200 kV accelerating voltage. Disk or tube samples (30−150 μM) were deposited on the copper grids for 1 min, rinsed twice using pure water, and dried by nitrogen blowing. Samples on the copper grids were negatively stained with sodium phosphotungstate prior to TEM detection.

Enzyme Analysis of GPx Mimic of TMVcp Mutant. The GPx activities of enzymes were assayed by a coupled reductase method as described.[40] The reaction system was a 500 μL of solution containing 50 mM phosphate buffer, pH 7.0, 1 mM EDTA, 1 mM GSH, 1 U of glutathione reductase, 0.25 mM NADPH, and appropriate GPx mimics at 37 °C. Reaction was initiated by the addition of 0.5 mM H_2O_2 and the absorbance was recorded at 340 nm (ε = 6220 M^{-1} cm^{-1}, pH 7.0) using a Shimadzu UV-2450 UV−vis spectrophotometer. The reaction rate in the absence of enzyme was measured and subtracted from the catalytic reaction. The activity unit is defined as the amount of the enzyme that catalyzes the turnover of 1 μmol of NADPH per min. The specific activity is described as $\mu mol \cdot min^{-1} \cdot \mu mol^{-1}$.

The kinetics determination for the reduction of H_2O_2 by GSH catalyzed by Se-TMVcp142Cys149Arg was conducted using the method described by Yu *et al.*[41] The initial rates were obtained by changing the concentration of one substrate and keeping the concentration of the other constant. The enzyme mimic of Se-TMVcp142Cys149Arg was preincubated with GSH, NADPH, and GSSG reductase for 3 min. The reaction was initiated by the addition of H_2O_2. Subsequently, the reaction rates were obtained at various concentrations of substrates following the subtraction of the nonenzyme reaction rate.

Antioxidation of GPx Mimic of Se-TMVcp142Cys149Arg Disks or Tubes. Se-TMVcp142Cys149Arg assembled disks or tubes were assayed in the antioxidative research.[42] Specifically, the mitochondria swelling and the lipid peroxidation were determined in the protection of mitochondria against radical damage, according to the method previously described.[43,44]

Conflict of Interest: The authors declare no competing financial interest.

Acknowledgment. We thank M.B. Francis for the expression plasmid containing the gene of tobacco mosaic virus coat protein and A. Bock for the cysteine auxotrophic expression system. This work was supported by the Natural Science Foundation of China (No: 21234004, 91027023, 20921003, 21004028) and 111 project (B06009).

Supporting Information Available: Purification results of Se-TMVcp142Cys149Arg, TMVcp142Cys149Arg, and TMVcp; optimized expression process of Se-TMVcp142Cys149Arg; MALDI-TOF mass spectrometry and ICP results of Se-TMVcp142Cys149Arg; AFM determinations of Se-TMVcp142Cys149Arg tubes at various concentrations; glutaraldehyde cross-linking of disks and tubes of Se-TMVcp142Cys149Arg; HPLC purification of the assemblies; activity assay of various GPx mimics; the GPx determination over pH range. This material is available free of charge *via* the Internet at http://pubs.acs.org.

REFERENCES AND NOTES

1. Carette, N.; Engelkamp, H.; Akpa, E.; Pierre, S. J.; Cameron, N. R.; Christianen, P. C.; Maan, J. C.; Thies, J. C.; Weberskirch, R.; Rowan, A. E.; *et al.* A Virus-Based Biocatalyst. *Nat. Nanotechnol.* **2007**, *2*, 226–229.
2. Rong, J. H.; Oberbeck, F.; Wang, X. N.; Li, X. D.; Oxsher, J.; Niu, Z. W.; Wang, Q. Tobacco Mosaic Virus Templated Synthesis of One Dimensional Inorganic-Polymer Hybrid Fibres. *J. Mater. Chem.* **2009**, *19*, 2841–2845.

3. Shenton, W.; Douglas, T.; Young, M.; Stubbs, G.; Mann, S. Inorganic−Organic Nanotube Composites from Template Mineralization of Tobacco Mosaic Virus. *Adv. Mater.* **1999**, *11*, 253–256.
4. Lee, Y. J.; Yi, H.; Kim, W. J.; Kang, K.; Yun, D. S.; Strano, M. S.; Ceder, G.; Belcher, A. M. Fabricating Genetically Engineered High-Power Lithium-Ion Batteries Using Multiple Virus Genes. *Science* **2009**, *324*, 1051–1055.
5. Witus, L. S.; Francis, M. B. Using Synthetically Modified Proteins To Make New Materials. *Acc. Chem. Res.* **2011**, *44*, 774–783.
6. Stephanopoulos, N.; Carrico, Z. M.; Francis, M. B. Nanoscale Integration of Sensitizing Chromophores and Porphyrins with Bacteriophage MS2. *Angew. Chem., Int. Ed.* **2009**, *48*, 9498–9502.
7. Schlick, T. L.; Ding, Z. B.; Kovacs, E. W.; Francis, M. B. Dual-Surface Modification of the Tobacco Mosaic Virus. *J. Am. Chem. Soc.* **2005**, *127*, 3718–3723.
8. Bruckman, M. A.; Soto, C. M.; McDowell, H.; Liu, J. L.; Ratna, B. R.; Korpany, K. V.; Zahr, O. K.; Blum, A. S. Role of Hexahistidine in Directed Nanoassemblies of Tobacco Mosaic Virus Coat Protein. *ACS Nano* **2011**, *5*, 1606–1616.
9. Zahr, O. K.; Blum, A. S. Solution Phase Gold Nanorings on a Viral Protein Template. *Nano Lett.* **2012**, *12*, 629–633.
10. Wu, L.; Zang, J.; Lee, L. A.; Niu, Z.; Horvatha, G. C.; Braxtona, V.; Wibowo, A. C.; Bruckman, M. A.; Ghoshroy, S.; Zur Loye, H. C.; *et al*. Electrospinning Fabrication, Structural and Mechanical Characterization of Rod-Like Virus-Based Composite Nanofibers. *J. Mater. Chem.* **2011**, *21*, 8550–8557.
11. Katz, E.; Willner, I. Integrated Nanoparticle-Biomolecule Hybrid Systems: Synthesis, Properties, and Applications. *Angew. Chem., Int. Ed.* **2004**, *43*, 6042–6108.
12. Mao, C. B.; Solis, D. J.; Reiss, B. D.; Kottmann, S. T.; Sweeney, R. Y.; Hayhurst, A.; Georgiou, G.; Iverson, B.; Belcher, A. M. Virus-Based Toolkit for the Directed Synthesis of Magnetic and Semiconducting Nanowires. *Science* **2004**, *303*, 213–217.
13. Bruckman, M. A.; Liu, J.; Koley, G.; Li, Yu; Benicewicz, B.; Niu, Z. W.; Wang, Q. Tobacco Mosaic Virus Based Thin Film Sensor For Detection of Volatile Organic Compounds. *J. Mater. Chem.* **2010**, *20*, 5715–5719.
14. Miller, R. A.; Stephanopoulos, N.; McFarland, J. M.; Rosko, A. S.; Geissler, P. L.; Francis, M. B. Impact of Assembly State on the Defect Tolerance of TMV-Based Light Harvesting Arrays. *J. Am. Chem. Soc.* **2010**, *132*, 6068–6074.
15. Lin, Y.; Balizan, E.; Lee, L. A.; Niu, Z.; Wang, Q. Self-Assembly of Rodlike Bio-Nanoparticles in Capillary Tubes. *Angew. Chem., Int. Ed.* **2010**, *49*, 868–872.
16. Nam, Y. S.; Magyar, A. P.; Lee, D.; Kim, J. W.; Yun, D. S.; Park, H.; S.P., T., Jr; Weitz, D. A.; Belcher, A. M. Biologically Templated Photocatalytic Nanostructures for Sustained Light-Driven Water Oxidation. *Nat. Nanotechnol.* **2010**, *5*, 340–344.
17. Gorzny, M. L.; Walton, A. S.; Evans, S. D. Synthesis of High-Surface-Area Platinum Nanotubes Using a Viral Template. *Adv. Funct. Mater.* **2010**, *20*, 1295–1300.
18. Komatsu, T.; Terada, H.; Kobayashi, N. Protein Nanotubes with an Enzyme Interior Surface. *Chem.—Eur. J.* **2011**, *17*, 1849–1854.
19. Fang, Z. H.; Lu, L. M.; Zhang, X. B.; Li, H. B.; Yang, B.; Shen, G. L.; Yu, R. Q. A Third-Generation Hydrogen Peroxide Biosensor Based on Horseradish Peroxidase Immobilized in Carbon Nanotubes/SBA-15 Film. *Electroanal.* **2011**, *23*, 2415–2420.
20. Haratake, M.; Matsumoto, S.; Ono, M.; Nakayama, M. Nanoparticulate Glutathione Peroxidase Mimics Based on Selenocysteine-Pullulan Conjugates. *Bioconjug. Chem.* **2008**, *19*, 1831–1839.
21. Fu, J. L.; Liu, M. H.; Liu, Y.; Woodbury, N. W.; Yan, H. Interenzyme Substrate Diffusion for an Enzyme Cascade Organized on Spatially Addressable DNA Nanostructures. *J. Am. Chem. Soc.* **2012**, *134*, 5516–5519.
22. Wilner, O.; Shimron, S.; Weizmann, Y.; Wang, Z. G.; Willner, I. Self-Assembly of Enzymes on DNA Scaffolds: En Route to Biocatalytic Cascades and the Synthesis of Metallic Nanowires. *Nano lett.* **2009**, *9*, 2040–2043.
23. Wilner, O. I.; Weizmann, Y.; Gill, R.; Lioubashevski, O.; Freeman, R.; Willner, I. Enzyme Cascades Activated on Topologically Programmed DNA Scaffolds. *Nat. Nanotechnol.* **2009**, *4*, 249–254.
24. Bhabak, K. P.; Mugesh, G. Functional Mimics of Glutathione Peroxidase: Bioinspired Synthetic Antioxidants. *Acc. Chem. Res.* **2010**, *43*, 1408–1419.
25. Tang, Y.; Zhou, L. P.; Li, J. X.; Luo, Q.; Huang, X.; Wu, P.; Wang, Y.; Xu, J. Y.; Shen, J. C.; Liu, J. Q. Giant Nanotubes Loaded with Artificial Peroxidase Centers: Self-Assembly of Supramolecular Amphiphiles as a Tool To Functionalize Nanotubes. *Angew. Chem., Int. Ed.* **2010**, *49*, 3920–3924.
26. Epp, O.; Ladenstein, R.; Wendel, A. The Refined Structure of the Selenoenzyme Glutathione Peroxidase at 0.2-nm Resolution. *Eur. J. Biochem.* **1983**, *133*, 51–69.
27. Ge, Y.; Qj, Z. H.; Wang, Y.; Liu, X. M.; Li, J.; Xu, J. Y.; Liu, J. Q.; Shen, J. C. Engineered Selenium-Containing Glutaredoxin Displays Strong Glutathione Peroxidase Activity Rivaling Natural Enzyme. *Int. J. Biochem. Cell Biol.* **2009**, *41*, 900–906.
28. Maiorino, M.; Roche, C.; Kiess, M.; Koenig, K.; Gawlik, D.; Matthes, M.; Naldini, E.; Pierce, R.; Flohe, L. A Selenium Containing Phospholipid−Hydroperoxide Glutathione Peroxidsae in *Schistosoma Mansoni*. *Eur. J. Biochem.* **1996**, *238*, 838–844.
29. Zhu, Z. Q.; Ding, L.; Luo, G. M.; Liu, Z.; Sun, Q. A.; Yang, T. S.; Shen, J. C. Some Physicochemical and Enzymic Properties of Selenium-Containing Abzyme. *Biochem. Biophys. Res. Commun.* **1994**, *202*, 1645–1650.
30. Zhang, Y.; Li, Z. S.; Sun, M.; Zheng, Q. C.; Sun, C. C. Molecular Simulation Studies of A Selenium-Containing scFv Catalytic Antibody that Mimics Glutathione Peroxidase. *Biochim. Biophys. Acta* **2005**, *1747*, 27–34.
31. Seeliger, D.; de Groot, B. L. Ligand Docking and Binding Site Analysis with Pymol and Autodock/Vina. *J. Comput. Aided Mol. Des.* **2010**, *24*, 417–422.
32. Liu, X. F. Parameter Expansion for Sampling a Correlation Matrix: an Efficient GPX-RPMH Algorithm. *J. Stat. Comput. Simul.* **2008**, *78*, 1065–1076.
33. Makino, N.; Mise, T.; Sagara, J. Kinetics of Hydrogen Peroxide Elimination by Astrocytes and C6 Glioma Cells—Analysis Based on a Mathematical Model. *Biochim. Biophys. Acta* **2008**, *1780*, 927–936.
34. Ng, C. F.; Schafer, F. Q.; Buettner, G. R.; Rodgers, V. G. The Rate of Cellular Hydrogen Peroxide Removal Shows Dependency on GSH: Mathematical Insight into *in Vivo* H_2O_2 and GPx Concentrations. *Free Radic. Res.* **2007**, *41*, 1201–1211.
35. Dong, Z. Y.; Liu, J. Q.; Mao, S. Z.; Huang, X.; Yang, B.; Ren, X. J.; Luo, G. M.; Shen, J. C. Aryl Thiol Substrate 3-carboxy-4-nitrobenzenethiol Strongly Stimulating Thiol Peroxidase Activity of Glutathione Peroxidase Mimic 2,2′-Ditellurobis-(2-deoxy-β-cyclodextrin). *J. Am. Chem. Soc.* **2004**, *126*, 16395–16404.
36. Makino, N.; Sasaki, K.; Hashida, K.; Sakakura, Y. A Metabolic Model Describing the H_2O_2 Elimination by Mammalian Cells Including H_2O_2 Permeation through Cytoplasmic and Peroxisomal Membranes: Comparison with Experimental Data. *Biochim. Biophys. Acta* **2004**, *1673*, 149–159.
37. Mueller, H. S.; Senn, H.; Gsell, B.; Vetter, W.; Baron, C.; Bock, A. The Formation of Diselenide Bridges in Proteins by Incorporation of Selenocysteine Residues: Biosynthesis and Characterization of (Se)2-Thioredoxin. *Biochemistry* **1994**, *33*, 3404–3412.
38. Casi, G.; Roelfes, G.; Hilvert, D. Selenoglutaredoxin as a Glutathione Peroxidase Mimic. *ChemBioChem* **2008**, *9*, 1623–1631.
39. Dedeo, M. T.; Duderstadt, K. E.; Berger, J. M.; Francis, M. B. Nanoscale Protein Assemblies from a Circular Permutant of the Tobacco Mosaic Virus. *Nano Lett.* **2010**, *10*, 181–186.
40. Wilson, S. R.; Zucker, P. A.; Huang, R. R. C.; Spector, A. Development of Synthetic Compounds with Glutathione Peroxidase Activity. *J. Am. Chem. Soc.* **1989**, *111*, 5936–5939.

41. Yu, H. J.; Liu, J. Q.; Bock, A.; Li, J.; Luo, G. M.; Shen, J. C. Engineering Glutathione Transferase to a Novel Glutathione Peroxidase Mimic with High Catalytic Efficiency—Incorporation of Selenocysteine into a Glutathione-Binding Scaffold Using an Auxotrophic Expression System. *J. Biol. Chem.* **2005**, *280*, 11930–11935.
42. Yu, H. J.; Ge, Y.; Wang, Y.; Lin, C. T.; Li, Jing; Liu, X. M.; Zang, T. Z.; Xu, J. Y.; Liu, J. Q.; Luo, G. M.; *et al*. A Fused Selenium-Containing Protein with Both GPx and SOD Activities. *Biochem. Biophys. Res. Commun.* **2007**, *358*, 873–878.
43. Jiang, Z. H.; Arner, E. S. J.; Mu, Y.; Johansson, L.; Shi, J. M.; Zhao, S. Q.; Liu, S. J.; Wang, R. Y.; Zhang, T. Z.; Yan, G. L.; *et al*. Expression of Selenocysteine-Containing Glutathione S-Transferase in *Escherichia Coli*. *Biochem. Biophys. Res. Commun.* **2004**, *321*, 94–101.
44. Zhao, K. S.; Zhao, G. M.; Wu, D. L.; Soong, Y.; Birk, A. V.; Schiller, P. W.; Szeto, H. Cell-Permeable Peptide Antioxidants Targeted to Inner Mitochondrial Membrane Inhibit Mitochondrial Swelling, Oxidative Cell Death, and Reperfusion Injury. *J. Biol. Chem.* **2004**, *279*, 34682–34690.